Universal Li-Ion Cell Electro-Thermal Model

Richard Stocker, Asim Mumtaz, Paramjeet, Michele Braglia, Neophytos Lophitis

This paper describes and verifies a Li-ion cell electro-thermal model and the associated data analysis process. It is designed to be adaptable and give accurate results across all variations of operating conditions and cell design based only on time domain voltage, current and temperature measurements. The creation of this model required an analysis process ensuring consistency in expressing the underlying cell behavior. This informed a flexible modelling structure adaptable both to cell performance variations and the limitations of the available test data. The model has been created with a combined thermal and electrical approach enabling 1D nodal distribution adaptable to both cylindrical and prismatic cells. These features combine with an intelligent parameter identification process identifying model structure and parameterization across the usage range, adaptable to any Nickel-Manganese-Cobalt Li-Ion cell. It is designed to retain physical meaning and representation to each circuit element across the temperature operating range. The model is verified in several different operating conditions through representative automotive cycling on an 18650 cell and a BEV2 format prismatic cell, representing the extremes of automotive cell design. The consistency of the model parameters with real phenomena is also analyzed and validated against Electrochemical Impedance Spectroscopy data.

***Index Terms*— Lithium-Ion, battery cell, simulation, model, time domain**

I. INTRODUCTION

Simulated battery control strategy development necessitates a plant model representative of real battery behavior. This includes modelling nonlinear dependencies on parameters [1], [2] and a highly dynamic voltage response including a range of time constants spanning several orders of magnitude [2]–[4]. With rapid evolution of cell capabilities, having an easily calibrated model adaptable to different cells is essential for long-term usefulness. This is of particular importance for automotive conditions, in which cell sizes, formats and chemistries vary significantly [5]. An additional complication is that internal cell design parameters are effectively hidden states without employing potentially expensive cell dismantling and chemical analysis. Finally, the model must be sufficiently computationally efficient to be able to run in real time for Hardware-in-the-Loop (HiL) testing and allow for quick simulation of a variety of control strategies. These aspects are of importance for battery cell degradation analysis. Being able to model individual physical contributions to impedance within a cell provides a platform for these to be grouped and changed based on individual cell ageing mechanism evolutions, facilitating simulation of degradation and failure scenarios as part of a control system or vehicle level simulation. For this type of application, a large magnitude of simulations would be required, however sufficient detail of underlying cell physical behavior must be retained, necessitating a physically representative yet computationally efficient model. Another advantage of this approach is it would not limit to automotive but across applications using Li-Ion cells.

Currently there is no clear winner in the automotive industry for either chemistry or design. Li-Ion is an umbrella term for battery cells based on lithium intercalation however the active materials of both positive and negative electrodes can vary [5], [6] and this affects all aspects of cell behavior including energy capability, impedance and durability. For automotive applications the main positive electrode chemistry is Nickel-Manganese-Cobalt (NMC), used by VW group, Nissan-Renault and BMW. Tesla use Nickel-Cobalt-Aluminum (NCA), and have been discussed as using Lithium Ferro Phosphate (LFP) for their Chinese entry level vehicles [7]. Cell designs also vary, with 3 popular variants: Cylindrical, Prismatic and Pouch [8]. These a vary in size, with some manufacturers such as Tesla opting for a large amount of parallel small capacity cylindrical cells with others such as BMW using single strings of high capacity prismatic cells. The range of Li-ion cells to be modelled varies dramatically, and any model must be flexible enough to easily adapt and characterize the cells across this range to try different designs and configurations effectively.

Modelling approaches for Li-Ion cells can be classified into 3 main types: empirical, equivalent circuit, and physical [9]. Empirical models are simple models formulated directly by fitting relationships to test data [10]. They are easy to construct and adapt to new cells, and lead to fast executing models. They however lack the sophistication to deal with the dynamic effects of the cell, limiting their accuracy to steady state conditions. They also do not attempt to explain or differentiate the contributions of different effects within the cell, making them difficult to adjust for ageing, which would scale impedance contributions along different timescales independently depending on which ageing mechanism is dominant [3].

Physical models are the antithesis to empirical models, with the intention to model real physical cell behavior. There are a wide range of these available for Li-Ion cells, commonly based on variations of the DUALFOIL model [11], [12]. These approaches can be highly accurate, and importantly give physical meaning behind the voltage responses, making them consistent and representative over a range of usage conditions and in dynamic profiles. Their downside is the level and depth of information required to populate, which may not be available to independent BMS developers without expensive chemical and physical testing. Methods have been developed to reduce the requirements needed for parameterization [13], [14] and simulation time [15], [16]. These approaches themselves are complex, with inertia in adapting the models to different cell designs and across chemistries. For degradation estimation these models can be challenging as while there are extensions to the DUALFOIL model to allow for individual degradation mechanisms to be added such as Solid Electrolyte Interphase (SEI) layer formation [11], electrode degradation [17] and

Richard Stocker is with the Institute for Future Transport and Cities, Coventry University, Coventry, CV1 2JH, United Kingdom. He is also with the Horizon Scanning department, HORIBA MIRA, Nuneaton, CV10 0TU, United Kingdom.
Neophytos Lophitis is with the Faculty of Engineering, University of Nottingham, Nottingham, NG7 2RD. Email: Neo.Lophitis@nottingham.ac.uk
Paramjeet (no surname) and Michele Braglia are also with HORIBA MIRA Horizon Scanning.
Asim Mumtaz is with the Department of Physics, University of Liverpool, L67 7ZF, United Kingdom. Email:A.Mumtaz@liverpool.ac.uk
Richard Stocker is the corresponding author. Corresponding author information follows. Title: Energy Systems Innovation Lead (at HORIBA MIRA). Contact Email Richard.Stocker@Horiba-Mira.com. Contact Tel +442476355275. Address is given as HORIBA MIRA address.

lithium plating [18], a comprehensive addition of degradation is very complex and difficult to transfer across chemistries.

Equivalent circuit models (ECM) fill the spectrum between pure empirical and chemical models [19]. They can vary dramatically in their objectives and functionality, with some being simple and still largely empirical, while others incorporate electrochemical-principles in their design [20], [21]. Most approaches use variations of an RCR model, consisting of a resistor followed by a number of Resistor-Capacitor pairs which give the model dynamic voltage response to current [22]–[25]. These models can be designed to give a good balance between computational effort and accuracy [26], and the parameterization and model development process can be largely automated, making them easy to apply quickly to new cell geometries. In addition, models that have been shown to work on different electrode chemistries are similar [27].

When using an ECM approach, it is important to consider the underlying causes behind cell resistance. These are complex, being present in both electrodes, electrode surface layers [28], electrolyte [2], [4] and current collectors [29]. These contributions vary significantly in both magnitude and response time to current application [3], [4], and their dependency on usage conditions such as temperature, current and State of Charge (SoC) [1], [4], [21], [30]–[32]. It is important to link the equivalent circuit parameters to consistent physical effects to create a model consistent across the different operating regions of a cell, even if the underlying causes are not specified. When considering as a platform for degradation analysis this modelling approach also makes sense, as it allows for alteration of parameters for individual contributions to cell impedance, allowing for a more comprehensive alteration of dynamic behavior due to degradation, without having to model the underlying electrochemical degradation causes.

The optimum number of RC elements to get a good fit has been explored previously [25], [26] but often only at 1 temperature. With temperature the time constants and magnitudes of resistance contributions change [3], [4], [21], [24]. This paper shows that this must be considered, as cell temperature can affect the number of significant resistance contributions required to be modelled. To make a model represent consistent effects across a cells operating range, the equivalent circuit structure must change to reflect this.

Common techniques for ECM characterization are through using Electrochemical Impedance Spectroscopy (EIS) in the frequency domain [33], [34] or through analyzing cell relaxation curves in the time domain [3], [32], [35], with some techniques using both [36], [37]. Time domain testing has the advantage it can be incorporated into testing that would already be required for acquiring BMS data, eliminating additional overhead required for model characterizing.

In this paper, a model is explained combining an informed time domain measurement analysis process with a flexible equivalent circuit modelling structure, adaptable to optimize for the presence of significant resistance effects in each temperature region. This is supported by a parameterization process, that informs both the required electrical model structure and circuit parameters across the different operational regions of the analyzed cell. During this work it was found, based on interpretation of physical contributions to resistance,

that the structure of the electrical model should consider the capabilities of the input data and the changing characteristics of the cell. A single ECM structure may not be enough over the operating range, particularly when accounting for temperature. The novel electrical model is combined with a thermal model having geometrical structures corresponding to both cylindrical and prismatic formats. Both models are constructed to allow a 1D nodal distribution of the active materials of the cell, chosen in the direction in which thermal gradients are most prominent.

The paper is structured as such: Section II defines the data processing and modelling approach. Section III shows this approach applied to an example BEV2 format cell, explaining the model structure in section II. Section IV verifies the model results electrically across a range of conditions and cross-validates circuit model conclusions through EIS measurements. Conclusions are summarized in section 0.

II. MODEL AND DATA ANALYSIS APPROACH

A. Model Architecture

The model architecture, shown in Fig. 1, is a closed loop interaction between electrical and thermal submodules with a defined interface. This allows flexibility to modify thermal or electrical models in isolation. All modules in this paper were developed using Matlab/Simulink [38]. It is important to consider both the electrical and thermal behavior of the cell due to their interaction effects. Cell resistance, capacity and Open Circuit Voltage (OCV) [35] as electrical characteristics all depend on the temperature of the active materials of the cell, so to be expressed across the cell's operating range an accurate representation of this temperature is needed for correct estimation of load voltage and SoC. The reversible (entropic) and irreversible (joule) heating of the cell are dependent on the SoC and load voltage drop of the cell, so need to respond to the changes in electrical characteristics. This has been accounted for in the overall model by coupling the electrical and thermal models, allowing for the thermal model to adapt to the electrical characteristics SoC and voltage drop, and for the electrical model to respond to changes in active material temperature.

Recent research in battery cell behavior, particularly for large, energy dense cells used in some automotive applications, shows electrical and thermal states can vary throughout cell thickness [12], [39]–[41]. In extreme cases this causes differences in lithiation across the active material 'jellyroll' [42], affecting cell performance and lifetime [41]. To account for this, a 1D nodal distribution is incorporated into the electrical and thermal models. An explanation of the underlying approach is provided in our previous publication [25].

B. Thermal Model

The Thermal model is based around an energy balance approach shown in (1), which shows net power transfer to an
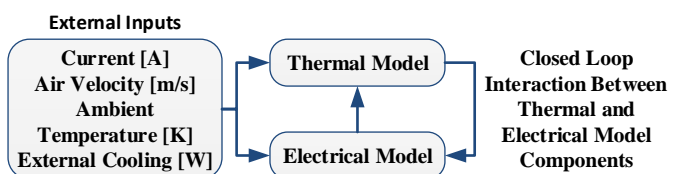

Fig. 1 Model interactions and interface. Adjusted from [25] .

active material node based on four main power contributions for the cell. This is used in conjunction with the cell mass m_{node} and specific heat Cp_{node} characteristics, to calculate temperature change over a given timestep. The power terms consist of irreversible joule heating $\dot{q}_{ir}$, reversible entropic power transfer $\dot{q}_e$, convection between the cell and environment $\dot{q}_c$ and power transfer due to external cooling $\dot{q}_{ex}$. The thermal model has been explained previously in [25].

Irreversible heat generation is modelled using the resistance input from the electrical model (2). Reversible entropic thermal power transfer is modelled by (3) [12], [43]. An exposed cell thermally interacts with the environment through convective effects, modelled by (4). This general equation has been used in models previously [40], [44]. The cell surface convection coefficient is modelled using known properties of air, taken from [45], and relations for natural and forced convections for either flat surfaces or cylinders, depending on cell geometry [46]–[49]. The final term included in the heat balance is external cooling, allowing simulation of power transfer from external thermal management systems.

With the thermal model being largely based on physical laws, the information required for cell variation is low, requiring only cell geometry, specific heat capacity, thermal conductivity and entropic coefficient. Specific heat capacity and thermal conductivity can be acquired through simple, well known tests, manufacturer data or literature [44], [50]. The entropic coefficient can be empirically calculated through analyzing change in open circuit voltage with temperature, as a function of SoC [40], [43], [44], [49], [51], [52]. As this would require very accurate true OCV readings across the measurement range, the values representative for NMC/graphite were taken from a literature example that performed extensive testing [53]. For the convection part of the model, several fluid properties were required for air, which were taken from [45].

$$m_{node}Cp_{node}(T_N\text{-}T_{N\text{-}1})=\dot{q}_{ir}+\dot{q}_{ex}\text{-}\dot{q}_c\text{-}\dot{q}_e \tag{1}$$

$$\dot{q}_{ir}=I^2R \text{ [W]} \tag{2}$$

$$\dot{q}_e=T_{cell}\Delta S=\text{-}T_{cell}I\left(\frac{\delta V_{oc}}{\delta T}\right) \tag{3}$$

$$\dot{q}_c=h_sA_s(T_s\text{-}T_a) \tag{4}$$

C. Electrical Model

An ECM approach was used for the electrical model for reasons discussed in section I. The novelty of the approach is the variance of the number of elements within the circuit. This can either be 2RC or 3RC, depending on the current temperature the battery cell is operating within. The approach to transition between circuits is to gradually reduce/increase the relevant RC element resistance from a known value in the 3RC range, to zero in the 2RC range, while correspondingly scaling the capacitance to maintain the time constant between the temperature thresholds defining 2RC and 3RC usage.

The parameters for each element change with operating conditions, based temperature, SoC and applied current [54], [55]. OCV depends heavily on SoC, and has mild dependence on temperature [35]. There is a strong hysteresis effect of open circuit voltage with current history [44], [56] with true OCV

only occurring after several hours [57]. To account for hysteresis, separate 2D OCV maps were implemented for charge and discharge. A hysteresis function allows for gradual transition to the true OCV using the approach shown in [55].

Alongside the model, an approach has been used for parameterization to individual cell performance attributes and to define the regions in which each model structure should be used, as shown in Fig. 2. This approach uses curve fitting of cell relaxation behavior through a least square regression fit. This approach initially characterizes the cell through individual relaxation data points. Curve fitting however does not guarantee physical representation in its results. To account for this, all datapoints at a given temperature are then compared to ensure a consistent trend for each component. This process is done on each datapoint using (5) for the 2RC curve and (6) for the 3RC curve. The trends for each circuit are then analyzed, to identify signs of over/under fitting and identify circuit is suitable for each region. Analysis is performed to understand what the curve fitting has identified and the model structure we should use across the temperature range. If the process is evaluated only from the RMSE of the curve fitting itself, an equivalent circuit model with more elements could give more accurate fits to individual data points, but at the expense of losing the relationship to real physical/chemical phenomena. This can cause inconsistency in the resultant maps used to express circuit element values across the model, which would increase uncertainty between characterized points and remove correlation to real behavior.

$$V_{sim} = \left(1 - \exp\left(\frac{-t}{R_1C_1}\right)\right)I_{cell}R_1 + \left(1 - \exp\left(\frac{-t}{R_2C_2}\right)\right)I_{cell}R_2 \tag{5}$$

$$V_{sim} = \left(1 - \exp\left(\frac{-t}{R_1C_1}\right)\right)I_{cell}R_1 + \left(1 - \exp\left(\frac{-t}{R_2C_2}\right)\right)I_{cell}R_2 + \left(1 - \exp\left(\frac{-t}{R_3C_3}\right)\right)I_{cell}R_3 \tag{6}$$

III. DATA ANALYSIS APPLIED TO BEV2 CELL RESULTS

In this section, the data analysis and equivalent circuit construction approach is explained using the characterization results for an automotive grade BEV2 cell, showing how data analysis was used to define the novel equivalent circuit structure transition with temperature. Characterization testing was performed at several temperature intervals between -25°C and +40°C. The model was characterized used a combination of pulses and relaxations across a range of current, SoC and temperature values, similar to that used in [55], [58] under temperature control conditions that kept the cycled cell within 3°C of test target temperature in each case. This have a range of usable data to perform the curve fitting and modelling approach and analyze the results.
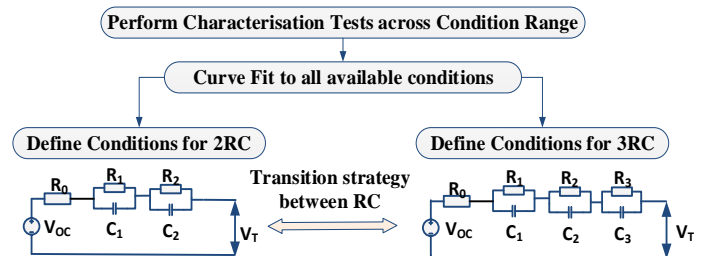

Fig. 2 Process for combining 2RC and 3RC Model

To decide the ECM structure transition with temperature, it was important to find how the time constants varied, and how many effects were visible to analyze. Ohmic losses are caused by the material resistance of the active materials [59], current collectors [29] and electrolyte. Ohmic resistance can be treated as instantaneous so does not need a capacitive effect modelled but has some temperature dependence due to the changes in conductivity of the electrolyte. Charge transfer impedance happens at the interfaces between materials, and therefore can occur at the surfaces of both electrodes, and the SEI layer. This has a capacitive element and is therefore time dependent, but particularly for the SEI and anode can act very quickly which may make it impossible to model effectively with practical data [2], [4]. Charge transfer has a very strong temperature dependence in both time constant and resistance magnitude [4], [21], [24] as well as a characteristic exponential dependence on SoC [4], [21]. Impedance is also found opposing the diffusion of Li-ions within the electrode and electrode bulk active materials. These act over much slower time scales than other effects, meaning they are will always be modelled as a dynamic effect with capacitance [2], [4]. Between different cell designs, the magnitudes and time constants of these effects vary. We know however that ohmic resistance will always be instantaneous, and diffusion will always have visible dynamic behavior. To adapt the structure for each individual cell model therefore, two aspects must be investigated. The first is if the diffusion and charge transfer behaviors are distinct enough to be seen separately, and the second is if the charge transfer resistance has a long enough time constant to be appropriately modelled from the characterization data. As all resistance effects are strongly temperature dependent, this must be analyzed across the temperature range to see how the appropriate modelling structure changes.

` The first step in this process was analyzing the resistance results in the first observable datapoint after current is removed. In this case after 5ms due to the 200Hz frequency range. This gives information on the resistance contributions that have already evolved in this phase, and therefore will not be possible to quantify for the dynamic equivalent circuit elements. If the effects cannot be quantified in the time resolution applied, then modelling them will not improve accuracy or physical representation of the system for the target applications. Once this is performed, the dynamic results of the curve fitting are interpreted to identify parameter trends and `consistency between different temperature points. The analysis of the available information is then used to define on the ECM structure across the parameter range to ensure consistency.

First timestep resistance with SoC relative to the maximum at that temperature across a range of temperatures at C/10 discharge are shown in Fig. 3. The charge results showed similar trends. The following can be observed:

1. At very low temperatures <10°C, the first timestep resistance is virtually independent of SoC.
2. At higher temperatures, a trend forms in which resistance rises exponentially as SoC approaches zero.

The relative independence of SoC below 0°C suggests almost exclusively ohmic and SEI resistance contributions, known to be SoC independent [4], [21]. As temperature rises the first timestep has an additional, SoC dependent contribution. This
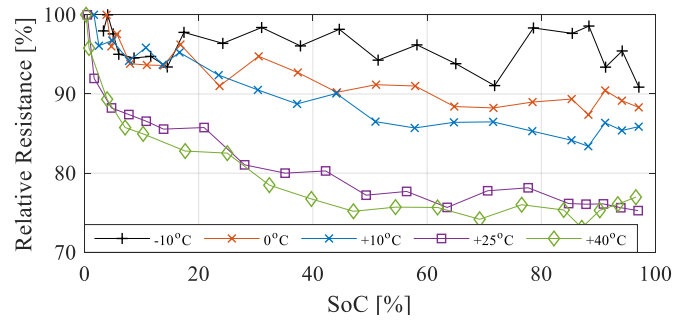

Fig. 3 Discharge First Timestep C/10 Resistance relative to maximum resistance with SoC at various temperatures

becomes apparent at 0°C and dominates at 25°C. This shows the characteristic shape of charge transfer resistance of one or both electrodes, which has a relatively fast time constant and exponential increase at low SoC during discharge[2], [3], and a strong temperature dependence [4], [21], [24]. Specifically, it decreases in magnitude and time constant with temperature.

This has model structure implications. Because the first timestep is not always just ohmic, but also including charge transfer, the single resistor cannot be modelled independently of SoC. The second, is that at low temperatures it is not present in the first timestep, suggesting it is detectable in the dynamic curve fitting analysis. As temperature increases it increasingly shifts to a frequency undetectable by the testing sample rate. At higher temperatures therefore, less effects will be sufficiently dynamic for observation in the curve fitting analysis.

Fig. 4 highlights when charge transfer significantly shifts into the first timestep through showing a linear decrease in first timestep resistance until 283K (10ºC) at a consistent SoC of 80%. Above 10ºC, the trend reduces, indicating further reductions of ohmic resistance offset by increased presence of charge transfer in the first timestep. The trend suggests between 10ºC and 25 ºC is when charge transfer is significantly harder to detect within the testing data measurement resolution due to its faster time constant and lower resistance.

The curve fitting process was performed across the temperature, SoC and current range using both 3RC and 2RC circuit architectures, shown in Fig. 2. Fig. 6 shows results for C/10 at -10ºC and 40 ºC for the 2RC and 3RC circuit structures.

When comparing the -10ºC data, the 2RC curves do not show distinct ties to a specific physical condition. It can be seen, that particularly for Time Constant of RC1 that over the SoC range it spans multiple orders of magnitude (0.5s to 20s). An increase in resistance and time constant is observed at around 60% SoC, a sign of anode solid state diffusion [30]–[32] influencing heavily both RC curves. It is also found that even when optimized, the 2RC approach cannot generate a sufficiently
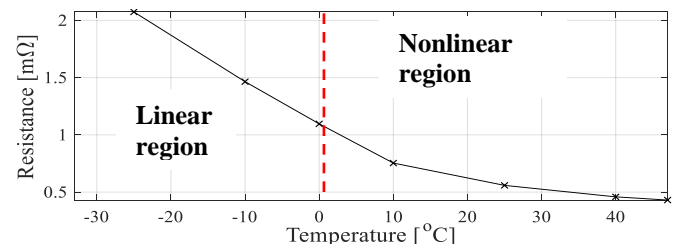

Fig. 4 First timestep resistance evolution with temperature at 80% SoC, 12A discharge BEV2 cell
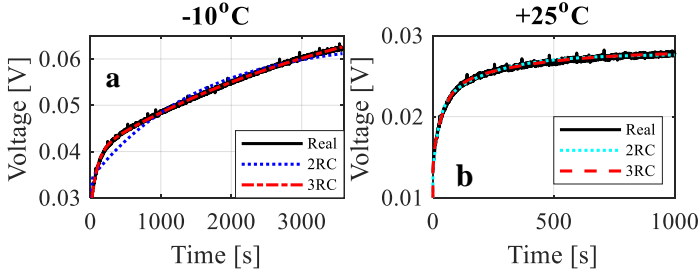
Fig. 5 Curve Fit Results in a mid-range SoC pulse with 2RC and 3RC circuits for (a) -10 ºC and (b) +25 ºC

accurate fit, suggesting it is not modelling all cell resistance contributions, as shown in Fig. 5.

In contrast to this, the 3RC approach shows a sufficiently good fit. Time constants of each RC circuit appear to be distinct orders of magnitude. The fast acting time constant of RC1 is not visible in the 2RC results, and is a good candidate for charge transfer due to its low SoC increase and time constant around 0.1s [2], [3]. The RC2 time constant shows relatively low sensitivity to SoC, which combined with its time constant range could be electrolyte or positive electrode diffusion [2]. The RC3 time constant shows the peak of between 50%-60%, which combined with the long time constants is a sign of solid state diffusion in the anode [30], [31]. The time constants show consistency and logical causes, suggesting 3RC is more suitable in this region. In the region of suspected anode phase change, there is a slight influence on the second time constant, indicating an area this process can be improved in the future.

At 40 ºC, the conclusions differ. The 3RC no longer gives a clear distinction between time constants. The time constant for RC1 spans more than one order of magnitude and does not show a clear trend with SoC. The second time constant also varies across a larger range than previously. The 2RC fit now shows consistency in its first time constant, and the expected spike in the second time constant, suggesting representation of real physical effects. The first time constant shows the relatively flat resistance curve of either liquid diffusion or that of NMC, while the second shows the characteristic peak associated with graphite. This shows that the 2RC circuit is a better choice in

this region and that the time constant of the visible charge transfer resistance has decreased beyond that capable of being modelled from the characterization data.

Illustration of individual curve fits for 2RC and 3RC relaxation curves at -10°C and +40°C are shown in Fig. 5. At -10°C there is a noticeable improvement from 2RC to 3RC in the matching the real relaxation curve, particularly in the first 800 seconds. At +40°C this is not the case, with the 2RC results giving a slightly better fit than the 3RC. This further suggests that 2 dynamic effects are visible at higher temperatures, while at lower temperatures there are 3. This vindicates the approach to vary the ECM structure with temperature.

This conclusion is logical when considering the first timestep analysis showed an additional effect move into the first timestep range at higher temperatures. This same range is when the 3RC circuit loses consistency in its shortest time constant. It could be deduced therefore, that less physical effects are observable as temperature increases, so to keep the consistency of the model, the 3RC approach needs to transition to a 2RC approach to keep consistency across the operating range.

The first timestep analysis suggests transition between 10 ºC and 25 ºC. The resultant time constant evolution is shown in Fig. 7, which shows a comparison of the 2nd and 3rd RC time constants of the 3RC approach with the 1st and 2nd time constants of the 2RC approach at 40% SoC, 12A 40% SoC is chosen to eliminate the impact of the SoC extremes and the phase change region. We would expect all dynamic effects with Li-ion cells to act with lower time constants as temperature increases [3], [4], [21], [24]. This is true for the 3RC time constants until +10 ºC, and for the 2RC at 25 ºC. A consistent trend is shown by transitioning across this temperature range, and therefore this is the ECM structure developed for this cell.

IV. MODEL VALIDATION

A. Test Cells

Two automotive Li-ion cells were used for the verification testing, both of Nickel-Manganese-Cobalt (NMC)/Graphite chemistry. The selection consisted of a BEV2 format energy cell, also used in section III, and an 18650 cylindrical cell.

Resistance and Time Constant Trends for 2RC and 3RC Circuits at -10°C and +40°C
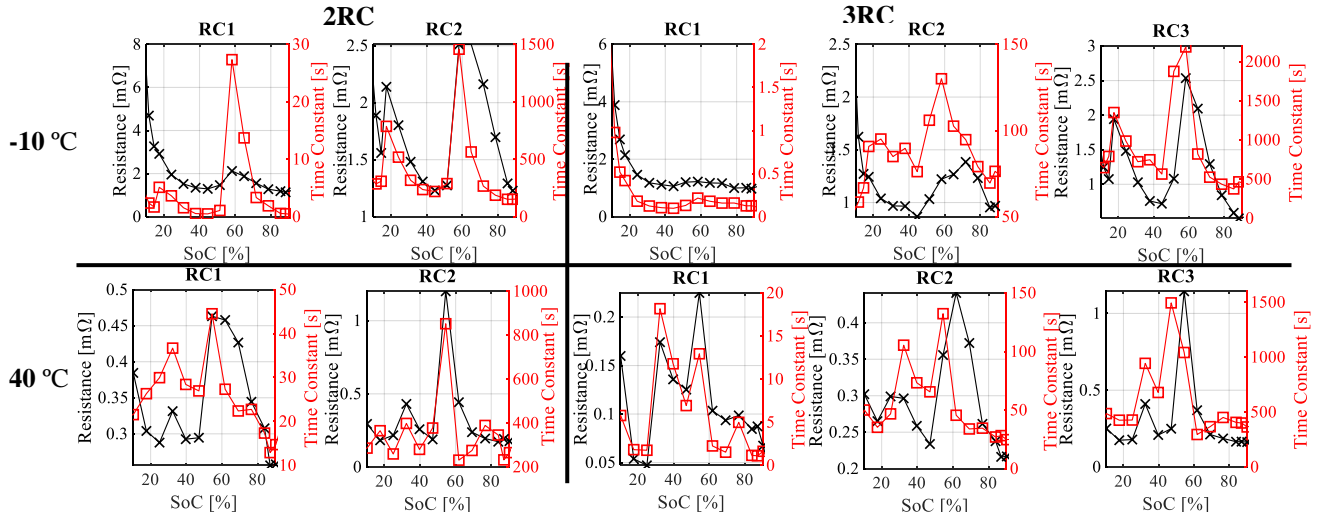

Fig. 6 BEV2 Discharge Resistance and Time Constant Results with SoC at -10°C and 40°C, 2RC and 3RC Circuit Structures
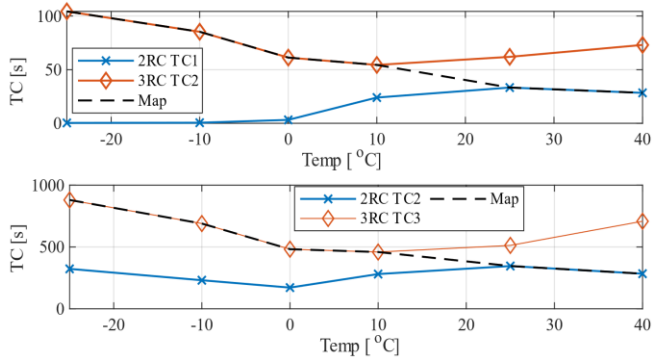
Fig. 7 3RC, 2RC and model trends with temperature.

These represent the two extremes of automotive cell design, showing the versatility of the presented approach.

B. Testing Approach

To support the modelling exercise, testing was performed both to parameterize the model and validate its output.

For validation testing, the BEV2 cell underwent four different test profiles, explained in *Table 1*. To test across the range of possible current magnitudes and directions, the first 3 tests used the Federal Urban Driving Schedule (FUDS), specified in [60]. The final test used a constant current charge. The temperatures were chosen to test a range of conditions, with 25ºC and 40ºC testing the 2RC section of the model, -10ºC the 3RC section, and the 5ºC test transitioning between the circuit setups. After all tests, relaxation was performed to allow the Open Circuit Voltage (OCV) to be compared between the simulation and test, gauging capacity accuracy. An additional test was then performed on the 18650 cell, using a Dynamic Stress Test (DST) [60] profile in ambient conditions at initially 25ºC to show the models applicability to smaller cells.

Electrical testing was temperature controlled through ambient temperature management and active thermal control, using a setup as shown in Fig. 8 to maintain temperature conditions at +/-3ºC throughout. For the thermal testing, cooling plates were not present, and the thermal chamber was switched off at test start. For all tests, the cell was soaked at initial test temperature at least 1 hour previously before testing.

C. Electrical/Thermal Model Testing Results

The tests are analyzed in the order in which they appear in Table 1. The results for test 1 are shown in Fig. 10, which show how the model performs over an individual FUDS cycle at 40ºC, starting from 95% SoC during temperature-controlled conditions. The model performs well, with the profile being

Table 1 List of Test Conditions

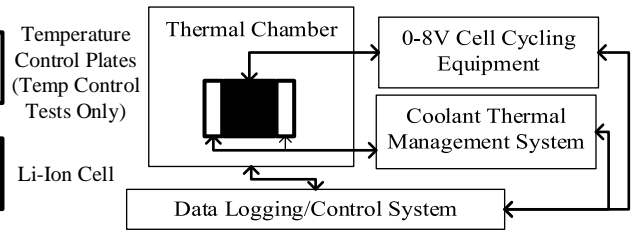| Test	1	2	3	4	5
Cell	BEV2	BEV2	BEV2	BEV2	18650
Initial Temp [ºC]	40 ºC	-10 ºC	25 ºC	5 ºC	25 ºC
Temp Control	Yes	Yes	No	No	No
Cycle Profile	FUDS	FUDS	FUDS	CC Charge	DST
Start SoC [%]	95	95	95	10	90
End Condition	1 FUDS cycle	V<3.5	V<3.5	V >4.115	16 FUDS cycles
Average Error [V]	0.0019	0.0057	0.0071	0.0041	0.0057

Fig. 8 Experimental Testing Setup Diagram

matched and simulation voltage being within 10mV of the test data across the test. The SoC and OCV correlation also seems to match well, with the relaxation at the end of the test being within 2mV. The mean error across the test was 1.9mV.

For test 2 FUDS cycling was performed at -10ºC across a large fraction of the SoC range, under temperature-controlled conditions starting from 95% SoC, shown in Fig. 9. It can be seen at low temperatures the voltage error can be larger during high current cycling, but the mean error was still low, at 5.7mV. After relaxation, the error reduced to approximately 3mV.

For test 3, the model had the additional task of estimating temperature. As we do not have a method for measuring internal temperature, the method of verification for temperature was to compare the expected temperature of the surface node, to that of the central temperature measurement of the cell. The results for voltage and temperature comparison are shown in Fig. 11. It can be seen the voltage comparison is very accurate, being within 20mV throughout (except for one instance) and average an error of 7.1mV. The model had an error of ~1.1mV after relaxation. Surface temperature matched well, with error <1ºC throughout, and a similar evolution profile.

Test 4 was designed to test the capability of the cell in two aspects. The first is being representative of a charging profile, in contrast to the driving profiles of the other tests, and the second is allowing the cell to heat up and transition between the 3RC and 2RC region of the testing. The results are shown in Fig. 12. The voltage profile matches well during the test, with the voltage within 15mV across the profile and an average error of 4.1mV, with a post-relaxation error of <1mV. The temperature had 1.2ºC maximum error.

The above tests were performed on a BEV2 format high energy prismatic cell. To test the adaptability of the model, an additional test was performed on an 18650 cylindrical cell through a Dynamic Stress Test (DST) cycle, in non-
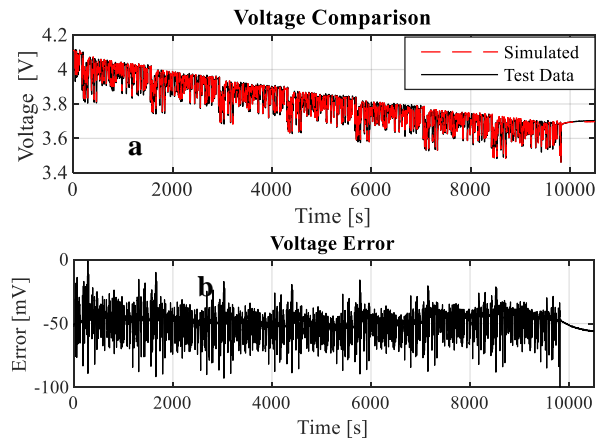

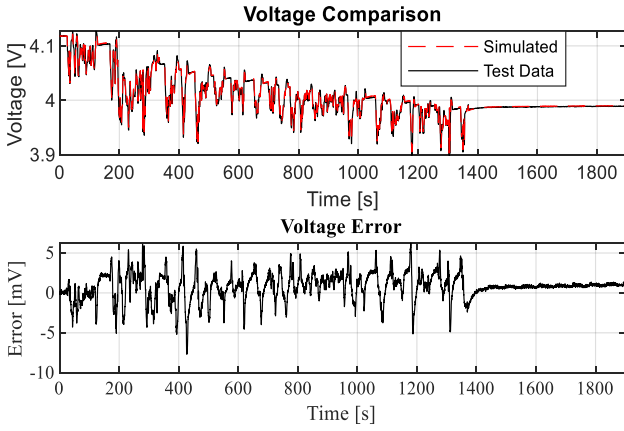*Fig. 9 Voltage Comparison (a) and error (b) test case 2*

Fig. 10 Voltage Comparison (a) and error (b) test case 1

temperature-controlled conditions starting at 25ºC. The results are shown in Fig. 13. It can be seen the voltage and temperature profiles match well. This test does not have extended relaxation data, but after 5800s (the last observable test point) the voltage error is approximately 5.7mV. The average test error is 5.7mV.

The results show that a small voltage error can be achieved across the temperature and SoC range, and that the approach can be applied to two vastly different cells.

D. Electrochemical Impedance Spectroscopy Results

The cell cycling testing proves model effectiveness, but a separate method is required to validate the individual equivalent circuit elements within the model. EIS testing was performed at 0ºC and 25 ºC across the frequency range of 10kHz-10mHz, at 3.6V (corresponding to approximately 30% SoC) under ambient temperature control conditions. These results were fitted to equivalent circuit models, with circuit characteristics compared to our time domain results. This data was then used

to fit to 3RC and 2RC circuits using ZView [61]. The results from the raw data and output from the ECM for 0 ºC and 25 ºC in Table 2 and illustrated in Fig. 14.

At 0ºC a 3RC circuit is necessary to give accurate results and each time constant is separated by at least one order of magnitude. At 25 ºC the 3RC approach was found to over-fit, with overlapping time constants, while the 2RC gave comparable accuracy, and a more physically representative fit. This is coherent with the time domain measurements (TDM) suggesting that the transition between the two-RC and the three-RC models is based on underlying physical behavior.

The time constant values of each RC parallel at each temperature are given in Table 2 for both the EIS and Time domain measurements. The frequency and time datasets do not cover the same range, but there is some overlap. Specifically, the frequency domain will find high frequency results that the time domain cannot identify, while the time domain can evaluate features with time constants beyond the largest EIS frequency, but the region of 200Hz to 10mHz (0.005s to 100s) will allow for observation from both techniques for comparison. These are shown as TC2 and TC3 in Table 2, which correspond to RC1 and RC2 in the time domain model. The time constants for EIS and time domain are comparable. It can also be seen, that at 25 ºC, the EIS time constant for TC2 is 0.01s, which would only be too fast for the time domain measurement, explaining why it is not detected, validating the removal of that RC element at 25 ºC and above.

V. Conclusions

This paper demonstrates the accuracy and flexibility of a compact, fast calculating equivalent circuit Li-ion cell model that can be developed across the range of cell designs and usage conditions expected in automotive applications. The influence
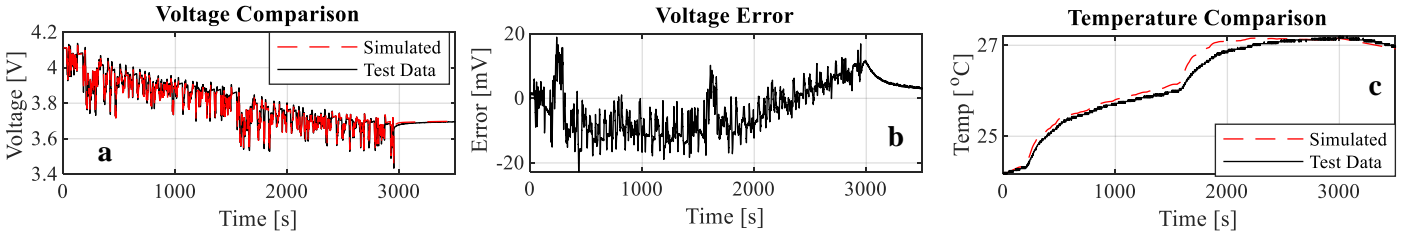

Fig. 11 Voltage Comparison (a) and error (b) test case 3. Surface temperature comparison in (c)
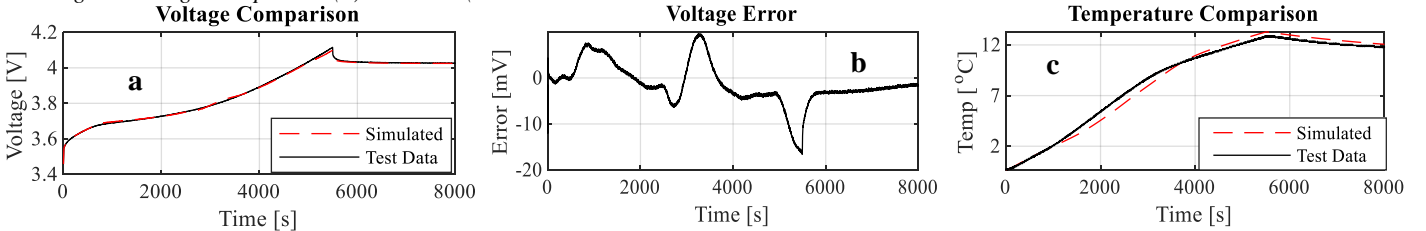

Fig. 12 Voltage Comparison (a) error (b) test case 4. Surface temperature comparison in (c).
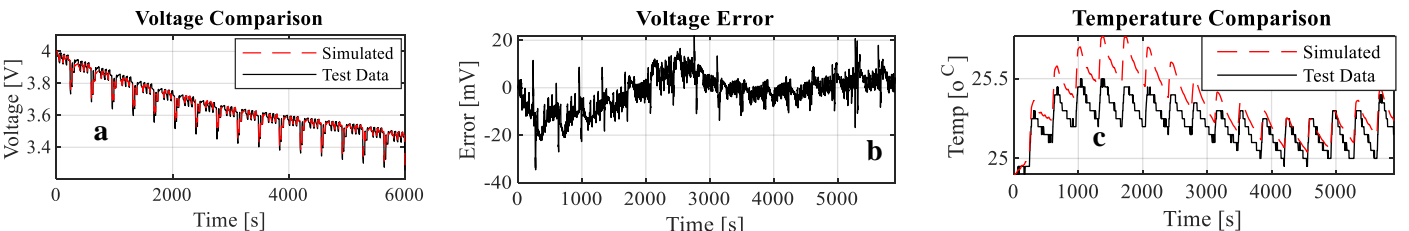

Fig. 13 Voltage Comparison (a) and error (b) test case 5. Surface temperature comparison in (c)

Table 2 EIS and TDM Results at 0 and 25ºC

Electrochemical Impedance Spectroscopy				
Temp [ºC]	TC1 [s]	TC2 [s]	TC3 [s]	TC4 [s]
0	0.0017	0.05	76	~
25	~	0.01	43	~
Time Domain Measurement				
Temp [ºC]	TC1 [s]	TC2 [s]	TC3 [s]	TC4 [s]
0	~	0.11	60.92	521.77
25	~	~	37.03	384.96

of temperature on the required modelling structure was shown as an essential consideration to give a representative emulation of important cell behavior across the temperature range. This was demonstrated by applying the data processing and modelling approach to two cells at the extremes of automotive design: an 18650 cell and a BEV2 format cell, both NMC/graphite chemistry. The model accuracy was shown through voltage and temperature test and simulation comparison during automotive representative highly dynamic drive cycles and constant current application across different temperatures. A discussion was had showing the physical justification of the model transition, which is the fact that while the ohmic and diffusion effects within a cell would follow the same model structure as temperature transitions, the fast acting and highly temperature dependent nature of charge transfer impedance leading to it being possible to model dynamically at low temperatures, yet appearing resistive at higher temperatures, requiring a consequent change in model structure.

It was shown that the maximum mean voltage error while testing the BEV2 and 18650 cell was <10mV and that the voltage and temperature profiles matched well those of the real cell. In addition to accuracy, physical consistency in the circuit elements was an important part of the modelling approach. This was tested by comparing the simple time domain approach used for our modelling, with frequency domain EIS data to compare the time constant values of the derived RC pairs. It was found that both approaches give similar results, with the time domain data finding an additional long timescale resistance effect.

The findings of this modelling process are important, as it shows that a single methodology, encompassing a testing, analysis and modelling process, can be applied across the range of automotive cell formats and usage environments. What is shown however, is that for this to be performed, a detailed physical understanding is required alongside the mathematical analysis, to identify which features are necessarily expressed at given temperature points for each cell, to ensure a physical underpinning and associated consistency when evaluating parameter changes across the operating range. With this being

Fig. 14 EIS Results and ECM Approach at 0ºC and 25 ºC

achieved, there can be confidence in using this platform as part of larger vehicle modelling, energy efficiency simulations and developing advanced control strategies requiring accurate representation of dynamic voltage behavior across a wide range of design conditions and usage scenarios.

VI. REFERENCES

[1] J. Philipp, S. Arnold, A. Loges, D. Werner, T. Wetzel, and E. Ivers-tiffée, "Measurement of the internal cell temperature via impedance : Evaluation and application of a new method," *J. Power Sources*, vol. 243, pp. 110–117, 2013.

[2] M. Schönleber, C. Uhlmann, P. Braun, and A. Weber, "A Consistent Derivation of the Impedance of a Lithium-Ion Battery Electrode and its Dependency on the State-of-Charge," *Electrochim. Acta*, vol. 243, pp. 250–259, 2017.

[3] S. Gantenbein, M. Weiss, and E. Ivers-ti, "Impedance based time-domain modeling of lithium-ion batteries : Part I," *J. Power Sources*, vol. 379, no. September 2017, pp. 317–327, 2018.

[4] D. Andre, M. Meiler, K. Steiner, C. Wimmer, T. Soczka-guth, and D. U. Sauer, "Characterization of high-power lithium-ion batteries by electrochemical impedance spectroscopy . I . Experimental investigation," *J. Power Sources*, vol. 196, no. 12, pp. 5334–5341, 2011.

[5] P. Miller, "Automotive lithium-ion batteries," *Johnson Matthey Technol. Rev.*, vol. 59, no. 1, pp. 4–13, 2015.

[6] A. Dinger *et al.*, "Batteries for Electric Cars: Challenges, Opportunities, and the Outlook to 2020," Düsseldorf, 2010.

[7] P. Lima, "Tesla's smart battery strategy in China," *PushEV's*, 2020. [Online]. Available: https://pushevs.com/2020/03/02/teslas-smart-battery-strategy-in-china/. [Accessed: 03-Mar-2020].

[8] R. Schröder, M. Aydemir, and G. Seliger, "Comparatively Assessing different Shapes of Lithium-ion Battery Cells," *Procedia Manuf.*, vol. 8, no. October 2016, pp. 104–111, 2017.

[9] R. Spotnitz, "Challenges for Battery Modeling," in *Advanced Automotive Battery Conference Europe 2016*, 2016.

[10] U. Seong, C. Burm, and C. Kim, "Modeling for the scale-up of a lithium-ion polymer battery," *J. Power Sources*, vol. 189, pp. 841–846, 2009.

[11] J. Christensen and J. Newman, "Cyclable Lithium and Capacity Loss in Li-Ion Cells," *J. Electrochem. Soc.*, vol. 152, no. 4, p. A818, 2005.

[12] A. Tourani, "Investigation into operating temperature effect on the performance of high capacity lithium-ion cells," Coventry University, 2013.

[13] A. Rahman, S. Anwar, and A. Izadian, "Electrochemical model parameter identification of a lithium-ion battery using particle swarm optimization method," *J. Power Sources*, vol. 307, pp. 86–97, 2016.

[14] A. Rodríguez, G. L. Plett, and M. S. Trimboli, "Improved transfer functions modeling linearized lithium-ion battery-cell internal electrochemical variables," *J. Energy Storage*, vol. 20, no. June, pp. 560–575, 2018.

[15] A. Seaman, T. Dao, and J. Mcphee, "A survey of mathematics-based equivalent-circuit and electrochemical battery models for hybrid and electric vehicle simulation," *J. Power Sources*, vol. 256, pp. 410–423, 2014.

[16] Y. Li, M. Vilathgamuwa, T. Farrell, S. Shing, N. Tham, and J. Teague, "A physics-based distributed-parameter equivalent circuit model for lithium-ion batteries," *Electrochim. Acta*, vol. 299, pp. 451–469, 2019.

[17] J. Christensen, "Modeling Diffusion-Induced Stress in Li-Ion Cells with Porous Electrodes," *J. Electrochem. Soc.*, vol. 157, no. 3, p. A366, 2010.

[18] N. Legrand, B. Knosp, P. Desprez, F. Lapicque, and S. Raël, "Physical characterization of the charging process of a Li-ion battery and prediction of Li plating by electrochemical modelling," *J. Power Sources*, vol. 245, pp. 208–216, 2014.

[19] A. Rahmoun and H. Biechl, "Modelling of Li-ion batteries using equivalent circuit diagrams," *Przegląd Elektrotechniczny*, vol. 2, no. 7, pp. 152–156, 2012.

[20] K. D. Stetzel, L. L. Aldrich, M. S. Trimboli, and G. L. Plett, "Electrochemical state and internal variables estimation using a reduced-order physics-based model of a lithium-ion cell and an extended Kalman filter," *J. Power Sources*, vol. 278, pp. 490–505, 2015.

[21] J. Illig, M. Ender, A. Weber, and E. Ivers-tiff, "Modeling graphite anodes with serial and transmission line models," *J. Power Sources*, vol. 282, pp. 335–347, 2015.

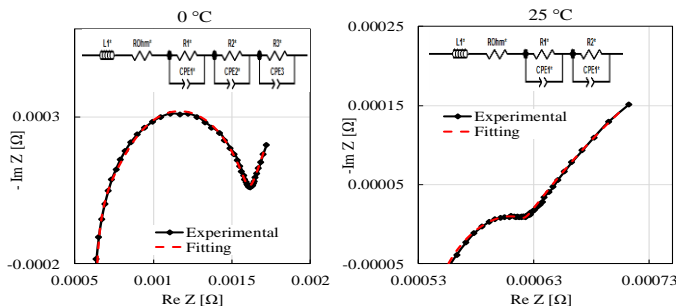[22] A. Marongiu, M. Roscher, and D. Uwe, "Influence of the vehicle-to-grid

strategy on the aging behavior of lithium battery electric vehicles," *Appl. Energy*, vol. 137, pp. 899–912, 2015.

[23] M. Abdel *et al.*, "Lithium-ion batteries : Evaluation study of different charging methodologies based on aging process," *Appl. Energy*, vol. 152, pp. 143–155, 2015.

[24] J. P. Schmidt, T. Chrobak, M. Ender, J. Illig, D. Klotz, and E. Ivers-tiffée, "Studies on LiFePO4 as cathode material using impedance spectroscopy," *J. Power Sources*, vol. 196, no. 12, pp. 5342–5348, 2011.

[25] R. Stocker, N. Lophitis, and A. Mumtaz, "Development and Verification of a Distributed Electro-Thermal Li-Ion Cell Model," in *44th Annual Conference of the IEEE Industrial Electronics Society (IECON)*, 2018, vol. 1, pp. 2044–2049.

[26] X. Hu, S. Li, and H. Peng, "A comparative study of equivalent circuit models for Li-ion batteries," *J. Power Sources*, vol. 198, pp. 359–367, 2012.

[27] A. Nikolian *et al.*, "Electrical Power and Energy Systems Complete cell-level lithium-ion electrical ECM model for different chemistries (NMC , LFP , LTO) and temperatures (− 5 ° C to 45 ° C) – Optimized modelling techniques," *Electr. Power Energy Syst.*, vol. 98, no. June 2017, pp. 133–146, 2018.

[28] I. A. J. Gordon *et al.*, "Electrochemical Impedance Spectroscopy response study of a commercial graphite-based negative electrode for Li-ion batteries as function of the cell state of charge and ageing," *Electrochim. Acta*, vol. 223, pp. 63–73, 2017.

[29] P. Taheri, A. Mansouri, B. Schweitzer, and M. Yazdanpour, "Electrical Constriction Resistance in Current Collectors of Large-Scale Lithium-Ion Batteries," *J. Electrochem. Soc.*, vol. 160, no. 10, pp. 1731–1740, 2013.

[30] M. Hess, "Kinetics and stage transitions of graphite for lithium-ion batteries," ETH Zurich, 2013.

[31] B. M. Winter, J. O. Besenhard, M. E. Spahr, and P. Novµk, "Insertion Electrode Materials for Rechargeable Lithium Batteries," *Adv. Mater.*, no. 10, pp. 725–763, 1998.

[32] J. V Persson, M. A. Danzer, M. Bauer, M. Wachtler, and H. St, "Understanding the dilation and dilation relaxation behavior of graphite-based lithium-ion cells," *J. Power Sources*, vol. 317, pp. 93–102, 2016.

[33] I. Meccanica, "Application of Li-ion cell ageing models on automotive electrical propulsion cells," Politecnico Di Milano, 2013.

[34] J. Illig, M. Ender, T. Chrobak, J. P. Schmidt, and D. Klotz, "Separation of Charge Transfer and Contact Resistance in LiFePO4-Cathodes by Impedance Modeling," *J. Electrochem. Soc.*, vol. 159, no. 7, pp. 952–960, 2012.

[35] C. R. Birkl, E. McTurk, M. R. Roberts, P. G. Bruce, and D. A. Howey, "A Parametric Open Circuit Voltage Model for Lithium Ion Batteries," *J. Electrochem. Soc.*, vol. 162, no. 12, pp. A2271–A2280, 2015.

[36] J. Illig, J. P. Schmidt, M. Weiss, A. Weber, and E. Ivers-tiffée, "Understanding the impedance spectrum of 18650 LiFePO4-cells," *J. Power Sources*, vol. 239, pp. 670–679, 2013.

[37] T. Bruen and J. Marco, "Modelling and experimental evaluation of parallel connected lithium ion cells for an electric vehicle battery system," *J. Power Sources*, vol. 137, pp. 511–536, 2015.

[38] I. The Mathworks, "MATLAB and Simulink 2015b." The MathWorks Inc, Natick, Massachusetts, USA, 2015.

[39] Y. Troxler *et al.*, "The effect of thermal gradients on the performance of lithium-ion batteries," *J. Power Sources*, vol. 247, pp. 1018–1025, 2014.

[40] R. Zhao, J. Liu, and J. Gu, "The effects of electrode thickness on the electrochemical and thermal characteristics of lithium ion battery," *Appl. Energy*, vol. 139, pp. 220–229, 2015.

[41] I. A. Hunt, Y. Zhao, Y. Patel, and G. J. Offer, "Surface Cooling Causes Accelerated Degradation Compared to Tab Cooling for Lithium-Ion Pouch Cells," *J. Electrochem. Soc.*, vol. 163, no. 9, pp. 1846–1852, 2016.

[42] M. Marinescu, B. Wu, M. Von Srbik, V. Yufit, and G. J. Offer, "The effect of thermal gradients on the performance of battery packs in automotive applications," in *Hybrid and Electric Vehicles Conference, IET*, 2013, pp. 1–5.

[43] T. M. Bandhauer, S. Garimella, and T. F. Fuller, "A Critical Review of Thermal Issues in Lithium-Ion Batteries," *J. Electrochem. Soc.*, 2011.

[44] A. Samba, "Battery Electrical Vehicles-Analysis of Thermal Modelling and Thermal Management," Universit´e de caen Basse Normandie; MOBI (the Mobility, Logistics and Au- tomotive Technology Research Centre), 2016.

[45] G. F. . Rogers and Y. . Mayhew, *Thermodynamic and Transport Properties of Fluids*, 5th ed. Oxford: Blackwell Publishing, 2010.

[46] S. W.Churchill and H. H.S.Chu, "Correlating equations for laminar and turbulent free convection from a vertical plate," *Int. J. Heat Mass Transf.*,

[47] S. W.Churchill and H. H.S.Chu, "Correlating equations for laminar and turbulent free convection from a horizontal cylinder," *Int. J. Heat Mass Transf.*, vol. 18, no. 9, pp. 1049–1053, 1975.

[48] University of Cairo, "Forced Convection Correlation," *Course MPE 635: Electronics Cooling*. Cairo University Faculty of Engineering, pp. 75–97, 2016.

[49] M. S. Rad, D. L. Danilov, M. Baghalha, M. Kazemeini, P. H. L. Notten, and E. T. Al, "Thermal Modeling of Cylindrical LiFePO4 Batteries," *J. Mod. Phys.*, vol. 4, no. July, pp. 1–7, 2013.

[50] V. Manuel *et al.*, "Thermal Analysis of a Fast Charging Technique for a High Power Li-Ion Cell," *batteries*, vol. 2, no. 4, pp. 1–9, 2016.

[51] S. Bazinski and X. Wang, "Determining Entropic Coefficient of the LFP Prismatic Cell at Various Temperatures and Charge/Discharge States," *ECS Trans.*, vol. 45, no. 29, pp. 85–92, 2013.

[52] C. Forgez, D. Vinh, G. Friedrich, M. Morcrette, and C. Delacourt, "Thermal modeling of a cylindrical LiFePO 4 / graphite lithium-ion battery," *J. Power Sources*, vol. 195, pp. 2961–2968, 2010.

[53] B. Manikandan, C. Yap, and P. Balaya, "Towards Understanding Heat Generation Characteristics of Li-Ion Batteries by Calorimetry, Impedance, and Potentiometry Studies," *J. Electrochem. Soc.*, vol. 164, no. 12, pp. A2794–A2800, 2017.

[54] W. Waag, S. Käbitz, and D. U. Sauer, "Experimental investigation of the lithium-ion battery impedance characteristic at various conditions and aging states and its influence on the application," *Appl. Energy*, vol. 102, pp. 885–897, 2013.

[55] C. Wu, R. Fu, Z. Xu, and Y. Chen, "Improved State of Charge Estimation for High Power Lithium Ion Batteries Considering Current Dependence of Internal Resistance," *Energies*, vol. 10, no. 10, p. 1486, 2017.

[56] P. Keil, S. F. Schuster, J. Travi, A. Hauser, R. C. Karl, and A. Jossen, "Calendar Aging of Lithium-Ion Batteries I . Impact of the Graphite Anode on Capacity Fade," *J. Electrochem. Soc.*, vol. 163, no. 9, pp. 1872–1880, 2016.

[57] L. Pei, T. Wang, R. Lu, and C. Zhu, "Development of a voltage relaxation model for rapid open-circuit voltage prediction in lithium-ion batteries," *J. Power Sources*, vol. 253, pp. 412–418, 2014.

[58] C. W. E. Fok, "Simulation of Lithium-Ion Batteries Based on Pulsed Current Characterization," The University of British Colombia, 2016.

[59] J. Illig, J. P. Schmidt, M. Weiss, A. Weber, and E. Ivers-tiffée, "Understanding the impedance spectrum of 18650 LiFePO 4 -cells," vol. 239, pp. 670–679, 2013.

[60] USABC, "Electric Vehicle Battery Test Procedures Manual Revision 2," 1996.

[61] D. Johnson, "Zview." Scribner Associates Inc, Southern Pines, North Carolina, USA, 2003.